Solution Structure of an Engineered Insulin Monomer at Neutral pH†

Helle B. Olsen,* Svend Ludvigsen, and Niels C. Kaarsholm

Novo Research Institute, Novo Nordisk A/S, Novo Allé 6A, DK-2880 Bagsvaerd, Denmark

Received February 7, 1996; Revised Manuscript Received April 22, 1996⊗

ABSTRACT: Insulin circulates in the bloodstream and binds to its specific cell-surface receptor as a 5808 Da monomeric species. However, studies of the monomer structure and dynamics in solution are severely limited by insulin self-association into dimers and higher oligomers. In the present work we use site-directed mutagenesis of the dimer- and hexamer-forming surfaces to yield the first insulin species amenable for structure determination at neutral pH by nuclear magnetic resonance (NMR) spectroscopy. The preferred insulin mutant, i.e., (B1, B10, B16, B27) Glu, des-B30 insulin retains 47% biological potency and remains monomeric at millimolar concentrations in aqueous solution at pH 6.5−7.5 as judged by NMR and near-UV circular dichroism (CD) spectroscopy. From a series of 2D ^{1}H-NMR spectra collected at pH 6.5 and 34 °C, the majority of the resonances are assigned to specific residues in the sequence, and nuclear Overhauser enhancement (NOE) cross-peaks are identified. NOE-derived distance restraints in conjunction with torsion restraints based on measured coupling constants, $^3J_{H^NH^\alpha}$, are used for structure calculations using the hybrid method of distance geometry and simulated annealing. The calculated structures show that the major part of the insulin mutant is structurally well defined with an average root mean square (rms) deviation between the 25 calculated structures and the mean coordinates of 0.66 Å for backbone atoms (A2−A19 and B4−B26) and 1.31 Å for all backbone atoms. The A-chain consists of two antiparallel helices, A2−A7 and A12−A19, connected by a loop. The B-chain contains a loop region (B1−B8), an α-helix (B9−B19), and a type I turn (B20−B23) and terminates as an extended strand (B24−B29). The B1−B4 and B27−B29 regions are disordered in solution. The structure is generally similar to crystal structures and resembles a crystalline T-state more than an R-state in the sense that the B-chain helix is confined to residues B9−B19.

Insulin is central to the hormonal control of metabolism. Due to its importance as a pharmaceutical preparation for the treatment of diabetes mellitus, much effort has been directed toward understanding the structural basis for insulin bioactivity. The protein is composed of two polypeptide chains, the A-chain (21 residues) and the B-chain (30 residues). The two chains are covalently linked by disulfide bridges at A7−B7 and A20−B19, and an intrachain disulfide bridge is joining A6 and A11. The three-dimensional structure of insulin has been characterized in detail by X-ray analysis of aggregated species, notably zinc insulin hexamers (Adams et al., 1969; Smith et al., 1984; Derewenda et al., 1989). The three principal hexamer conformations have been designated the T_6, T_3R_3, and R_6 forms, respectively (Kaarsholm et al., 1989). In each of these structures, the A-chain folds into a helix−loop−helix motif with helical stretches located in A2−A8 and A12−A19. The B-chain can assume two distinct conformations. In the T-state, the B-chain contains an extended N-terminal arm, a central α-helix (B9−B19), a type I turn (B20−B23), and a C-terminal β-strand. In the R-state, residues B1−B9 take up a helical conformation to form a region of α-helix contiguous from B1 to B19. The interconversion between the T_6, T_3R_3, and R_6 states of the insulin hexamer is modulated by a set of homotropic and heterotropic ligand binding interactions and has been shown to take place in solution (Kaarsholm et al., 1989; Brader et al., 1991; Bloom et al., 1995).

Although insulin hexamers are extensively characterized by X-ray crystallography, the physiologically active form of the hormone is the 5808 Da monomer. Hence, in any discussion of structure−activity relationships for insulin, it is necessary to consider whether crystal packing forces have modified the structure from that required for biological action. Due to the complicated pattern of insulin self-association in solution, detailed NMR[1] analysis of the insulin monomer has often been ambiguous. Accordingly, several groups have reported results of NMR studies carried out at low pH (i.e., pH 1.8−3.5) using either modified insulins, organic cosolvents, or both in an effort to counteract self-association [see, e.g., Kline and Justice (1990), Knegtel et al. (1991), Hua et al. (1991, 1992a, 1993b), Jørgensen et al. (1992), and Ludvigsen et al. (1994)]. The reported structures generally agree that the secondary structure of the insulin monomer in solution is similar to that of the crystallographically identified T-state. However, considerable differences are apparent in terms of the structural resolution expressed, e.g., by the atomic rms values.

In one extreme, insulin structures with properties similar to a "molten-globule" state have been reported. On the basis of these structures determined in the presence of 20% acetic acid, it has been postulated that the lack of tertiary structural detail is intrinsic to the native insulin monomer and that the

† The structures have been deposited at the PDB (file name 1HUI).

⊗ Abstract published in *Advance ACS Abstracts,* June 1, 1996.

[1] Abbreviations: NMR, nuclear magnetic resonance; CD, circular dichroism; COSY, two-dimensional correlated spectroscopy; DQF, double quantum filtered; DPI, des-(B26-B30); FID, free induction decay; NOE, nuclear Overhauser enhancement; NOESY, two-dimensional nuclear Overhauser enhanced spectroscopy; TOCSY, two-dimensional total correlation spectroscopy; rms, root mean square.

S0006-2960(96)00292-9 CCC: $12.00

phenomenon per se is important for the interactions of insulin with its receptor (Hua et al., 1991, 1992a,b, 1993a,b). In contrast with these low-resolution structures, our NMR studies on the biologically active B16 Tyr → His mutant in water at low pH have revealed a well-defined solution structure (Ludvigsen et al., 1994; Kaarsholm & Ludvigsen, 1995). Because the B16 His mutant remains essentially monomeric at millimolar concentrations in aqueous solution at low pH, these results identify sample homogeneity and aggregation state as major determinants for the quality of the NMR-derived structure.

The high-resolution solution structure of the insulin monomer at low pH provides an important prerequisite for the understanding of the interaction between insulin and its receptor. However, a long-term goal for these NMR studies is to determine the structure and dynamics of engineered monomers under physiological conditions as a base line for further structural examination of mutations associated with enhanced or diminished affinity for the insulin receptor.

Detailed NMR studies of the insulin monomer at neutral pH have so far been limited by protein solubility and self-association in addition to the inherently faster rate of NH exchange in this pH region. In the present work we use site-directed mutagenesis to manipulate the solubility and aggregation pattern of insulin in the neutral pH region. These experiments identify a mutant and a set of conditions where the monomer is amenable for high-resolution NMR structural analysis. The preferred mutant has glutamate residues substituted into four positions, i.e., B1 Phe, B10 His, B16 Tyr, and B27 Thr, and the C-terminal B30 Thr is removed. This mutant retains 47% biological potency and is monomeric at millimolar concentrations in the pH range 6.5−7.5. The resulting structure is generally well defined, as evidenced by a high number of sequential NOEs as well as many long-range NOEs. Apparent disorder is observed near the termini of the B-chain, e.g., B1−B4 and B27−B29, and is to a large extent ascribed to local effects of the mutations.

MATERIALS AND METHODS

Materials. Native and mutant insulins were constructed by oligonucleotide-directed mutagenesis, fermented in yeast, and purified as described (Markussen et al., 1987; Brange et al., 1988). In a typical small-scale preparation, the mutant is expressed and partly purified as a single-chain miniproinsulin precursor, B1...B29Lys-Ala-Ala-Lys-A1Gly...A21. Prior to the final purification step, the connecting peptide is cleaved off by treatment with a lysyl endopeptidase (*Achromobacter* protease I, EC 3.4.21.50; Wako Inc., Osaka, Japan), and the mutant insulin is isolated in the form of des-B30 Thr insulin. The removal of the B30 Thr residue has no effect on the biological potency of the molecule.

CD Spectroscopy. CD spectra were recorded with a Jobin Yvon Mark V dichrograph calibrated with (+)-10-camphorsulfonic acid as described (Kaarsholm et al., 1993). Near-UV CD spectra were recorded between 250 and 350 nm using an appropriate combination of cell path length and protein concentration to yield an absorbancy of less than 1. Protein concentrations were determined by UV absorbance using $\epsilon_{276} = 6.2 \times 10^3\ M^{-1}\ cm^{-1}$. The same extinction coefficient was used for estimation of the concentration of mutant species with the assumption that each of the four tyrosines in human insulin contributes 25% to ϵ_{276}.

NMR Spectroscopy. Samples were prepared by dissolving the lyophilized protein powder in 10/90 D_2O/H_2O or 99.8% D_2O and adjusting the pH as desired by additions of small amounts of 1 M DCl or NaOD. All pH meter readings are without correction for isotope effects. For all NMR experiments reported herein a temperature of 307 K was used.

Two-dimensional $^1H-^1H$ NMR spectra, DQF-COSY (Piantini et al., 1982; Rance et al., 1983), NOESY (Jeener et al., 1979; Anil-Kumar et al., 1980, 1981), and TOCSY (Braunschweiler & Ernst, 1983; Bax & Davis, 1985) were recorded on a Bruker AMX600 spectrometer. For TOCSY and NOESY spectra, mixing times were between 40−90 and 120−180 ms, respectively. All spectra had a spectral width in both dimensions of 6579 Hz; 1024 t_1 increments were acquired each with a size of 2048 real data points. The spectra were recorded in the phase-sensitive mode using the time-proportional phase incrementation scheme (TPPI; Marion & Wüthrich, 1983). The carrier was placed on the water resonance to enable irradiation of the water during a period of 1.5 s between the individual scans.

Prior to Fourier transformation the FID's were zero filled once in both dimensions. For processing of the DQF-COSY spectra, a squared sine-bell shifted 90° was used in both dimensions, whereas for the NOESY and TOCSY spectra, a Gaussian function with an exponential line broadening of −7 Hz and a factor of 0.15 was applied. Data processing was performed using the MNMR package (PRONTO Software Development and Distribution, Copenhagen, Denmark) or the Bruker UXNMR software on a Silicon Graphics Indigo computer. Exchange of amide protons was followed by a series of 8K data point one-dimensional spectra. These spectra were zero filled once, and a 1.5 Hz line broadening was used as a window multiplication prior to the Fourier transformation.

The program PRONTO [PRONTO Software Development and Distribution; see Kjaer et al. (1991)] was used to keep track of spectral assignments, cross-peak integration, sequence-specific and stereo-specific assignments, and related bookkeeping during spectral analysis. $^3J_{H^NH^\alpha}$ coupling constants were measured by the facility in the PRONTO software which uses a combined analysis of COSY and NOESY spectra (Ludvigsen et al., 1991). Chemical shifts were measured in parts per million as observed relative to dioxane (3.75 ppm).

Structure Calculations. The program X-PLOR (Brünger, 1992) was used to calculate structures based on distance and dihedral angle restraints derived from the NMR spectra. Integrated NOESY cross-peaks were divided into three classes of distance restraints using 1.0 Å as lower limit and upper limits of 2.7, 3.3, and 5.5 Å, respectively. For restraints involving methyl groups, an additional 0.5 Å was added to the upper limit. The measured $^3J_{H^NH^\alpha}$ coupling constants were converted into ϕ angle restraints as follows: $-60° \pm 30°$ (2−4 Hz); $-70° \pm 30°$ (4−6 Hz); $-120° \pm 60°$ (6−8 Hz); and $-120° \pm 35°$ (8−10 Hz). The stereospecific assignment of several β-methylene protons was obtained by combined analysis of COSY cross-peak patterns (Hybert et al., 1987) and of the intraresidual NOE intensities between the methylene protons and the α and the amide protons, respectively (Wagner et al., 1987). This method allowed assignment of the side chain to one of the three staggered conformations, χ_1, assuming the values $-60° \pm 60°$, $60° \pm 60°$, or $180° \pm 60°$. Stereospecific assignments of δ-methyl

groups of Leu residues were found and converted to χ_2 restraints in a similar fashion. The structure calculations were performed using a combination of distance geometry (Crippen & Havel, 1988; Kuszewski et al., 1992) and simulated annealing as proposed by Nilges et al. (1988).

Comparison of Solution Structures. From the Protein Data Bank (PDB), Brookhaven (January 1996), all files containing structures of monomeric native and mutant insulins determined by NMR were collected. Each file contains an ensemble of structures as well as a representative structure. For the purpose of comparison of the different structures, geometric average structures were calculated from these ensembles of structures following the alignment procedures presented in the literature references as listed in the header of the files. In order to obtain a reasonable comparison, we have made one exception to this procedure and used both chains rather than just the B-chain helix in the alignment of the DPI structures. Table 2 gives a summary of the experimental conditions and details concerning the structural calculations as referenced in the PDB files and in the original publications. The program X-PLOR (Brünger, 1992) was used to calculate the average structures.

RESULTS

Design of Monomeric Insulin Suitable for 2D NMR at Neutral pH. The aggregation and precipitation pattern of insulin is a complex function of protein concentration, pH, temperature, metal ions, ionic strength, and solvent composition. In the millimolar concentration range usually required for high-resolution NMR structural work, metal-free insulin exists predominantly as dimers and higher oligomers at pH 2.0−3.5. At higher pH aggregation increases, which in turn leads to precipitation in the pH region between 4.2 and 6.6. Above pH 6.6 insulin dissolves, presumably as a mixture of dimers and higher aggregates, which then gradually dissociate as the pH increases. As the pH is raised above 10−11, the monomeric state is finally reached (Jeffrey & Coates, 1966; Pekar & Frank, 1972; Lord et al., 1973; Goldman & Carpenter, 1974; Jeffrey et al., 1976; Pocker & Biswas, 1981; Strazza et al., 1985; Mark et al., 1987; Kaarsholm et al., 1990; Roy et al., 1990a; Kadima et al., 1992). The X-ray structure of the T_6 zinc insulin hexamer shows that distinct interfaces are involved in insulin dimer and hexamer packing (Baker et al., 1988). The published equilibrium constants for solution aggregation along the monomer/monomer interface are similar at pH 2 and 7 (i.e., $\approx 10^5$ M^{-1}). However, the corresponding aggregation along the dimer/dimer interface appears much stronger at pH 7 than at pH 2 (Mark et al., 1987). Hence, in contrast with the situation at low pH (Ludvigsen et al., 1994), insulin self-association must be inhibited along two distinct interfaces in order to obtain monomers at millimolar concentrations at neutral pH. At the same time, the resulting mutant should retain near-native biological potency, and the solubility pattern must allow NMR measurement in a pH range where the exchange rate of backbone NH protons is sufficiently slow for observation with conventional ^{1}H-NMR techniques (Wüthrich, 1986).

Aggregation properties of various insulin mutants were evaluated by near-UV circular dichroism (CD) and NMR resonance line widths. The near-UV CD spectrum (350−250 nm) of insulin reflects the environment of the tyrosine chromophore. The signal is very sensitive to aggregation and may be used to monitor the formation of dimer interface (Morris et al., 1968; Goldman & Carpenter, 1974; Wood et al., 1975; Strickland & Mercola, 1976). NMR spectra are sensitive to insulin self-association because longer rotational correlation times lead to line broadening and because dynamic equilibria between oligomeric states can lead to line broadening in the intermediate-exchange regime.

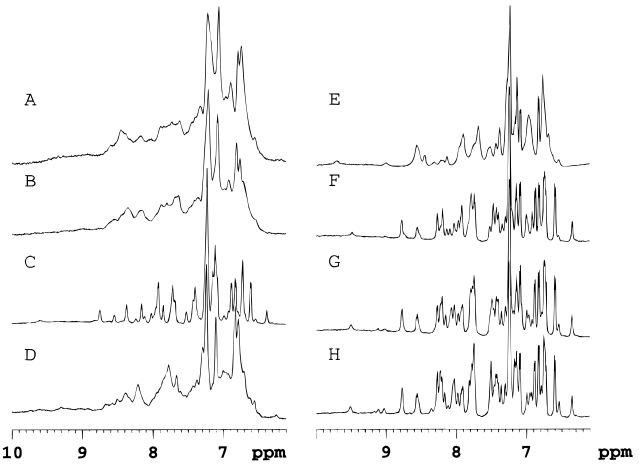

FIGURE 1: 1D NMR spectra showing the aromatic and amide proton resonances of native and mutant insulins at 1 mM protein concentration in 10/90 D_2O/H_2O, 307 K. Panels: (A) human insulin, pH 7.5; (B) B27 Thr → Glu, pH 7.5; (C) (B16, B27) Glu, pH 7.5; (D) (B1, B27) Glu, pH 7.5; (E) B10 Glu, des-B30, pH 7.5; (F−H) (B1, B10, B16, B27) Glu, des-B30 insulin at pH 7.5, 7.0, and 6.5, respectively.

Figure 1 shows the aromatic and amide proton resonances of the 1D ^{1}H-NMR spectra for human insulin (panel A) and a series of mutants (panels B−F) at 1 mM protein in 10/90 D_2O/H_2O, pH 7.5. Under these conditions, human insulin exists as a mixture of dimers and higher aggregates, and the resulting spectrum is very poorly resolved. The X-ray structure of the T_6 insulin hexamer shows that dimer formation is dominated by a series of nonpolar contacts contributed by B-chain residues, notably B12 Val and B16 Tyr in the central helix, and residues B23−B28 in the extended chain. Panels B and C illustrate the effects of introducing charged residues at two different positions in the monomer/monomer interface. As shown in panel B, the B27 Thr → Glu mutation at the edge of the monomer/monomer interface effects little or no improvement in spectral resolution relative to human insulin. This mutation has a minor inhibitory effect on dimer formation (Brange et al., 1988); however, in the present study the modification is preferred due to its positive effect on the expression level in yeast and hence on the overall fermentation yield during small-scale mutant preparation. Introduction of charge into the B16 Tyr position has previously been shown to provide an efficient means of inhibiting the formation of dimer interface at low pH (Ludvigsen et al., 1994; Kaarsholm & Ludvigsen, 1995). In accordance with this result, panel C shows that the B16 Tyr → Glu mutation strongly enhances the spectral resolution at pH 7.5. While the (B16, B27) Glu species is nearly monomeric at 1 mM protein, the exchange rate of several NH protons is too fast for observation in 2D spectra. At slightly lower pH, extensive line broadening is observed in concert with aggregation along the dimer/dimer interface. Accordingly, the number of cross peaks observed in 2D NOESY spectra of the (B16, B27) Glu mutant is

significantly smaller at pH 7.0 than at pH 7.5 (data not shown).

When the T_6 hexamer is assembled from dimers through the coordination of Zn^{2+} to the B10 His residues, both polar and non polar residues are buried between the dimers. The packing is correspondingly much looser than in the monomer/monomer interface within each dimer. A set of important contacts across the dimer-dimer interface involves the N-terminal part of the B-chain. Of particular interest is the B1 Phe residue, which fits into a pocket between the main A-chain and the A14 Tyr residue of its neighbor. Because the two A14 Tyr residues are also in contact across the dimer/dimer interface, a close aggregate involving four aromatic residues is formed (Baker et al., 1988). Comparison of panels B and D in Figure 1 shows that the B1 Phe → Glu mutation leads to somewhat improved resolution of the 1D NMR spectrum. A slightly better improvement is obtained with the B10 His → Glu mutation positioned at the edge of the dimer/dimer interface, viz. panel E.

The B10 His → Glu mutation also has the effect of increasing the biological potency of the insulin molecule 4-fold as determined by the ability to incorporate [2-^{3}H]-glucose in isolated mouse adipocytes according to Moody et al. (1974). In the same assay, the B27 Glu, (B1, B27) Glu, (B16, B27) Glu, and des-B30 insulins exhibit potencies of 1.07, 0.97, 0.13, and 1.00, respectively, relative to a value of 1.00 found for human insulin. For the mutant carrying all modifications, i.e., (B1, B10, B16, B27) Glu, des-B30 insulin, a relative potency of 0.47 is found, indicating that the substitutions affect the biological activity in a nearly independent manner. Panel F in Figure 1 shows that the 1D spectrum of (B1, B10, B16, B27) Glu, des-B30 insulin is well resolved and retains the dispersion of resonance lines characteristic for globular proteins. Furthermore, as the pH is adjusted down to 7.0−6.5, the high resolution is maintained (panels G and H), while selected NH resonances become sharper as expected due to the slowed exchange rate.

Figure 2 shows near-UV CD spectra as a function of protein concentration for native insulin at pH 8.0 and the (B1, B10, B16, B27) Glu, des-B30 mutant at pH 6.5 and 7.5. For native insulin, the progressive increase in intensity of the negative signal around 274 nm indicates the expected increase in association with increasing concentration. In contrast, the near-UV CD spectrum of the mutant is independent of the protein concentration in the 60 μM to 2.6 mM range at both pH 6.5 and 7.5. Although the mutant is missing one tyrosine reporter group (B16), Tyr B26 is expected to be strongly affected by monomer/monomer interactions. Hence, these results provide further evidence that the (B1, B10, B16, B27) Glu, des-B30 mutant is monomeric under conditions necessary for NMR structural studies at neutral pH, and this species was selected for detailed characterization.

Assignment of Spin Systems. NMR spectra were assigned using the standard procedures outlined by Wüthrich (1986). The fingerprint region of the DQF-COSY spectrum is shown in the upper panel of Figure 3. The chemical shifts are dispersed and well resolved as expected for a structured globular protein, and 37 of the 47 possible H^NH^α cross-peaks are annotated in the plot. Among the remaining H^NH^α cross-peaks, six were assigned using TOCSY spectra. These are the resonances that are either close to the water line or

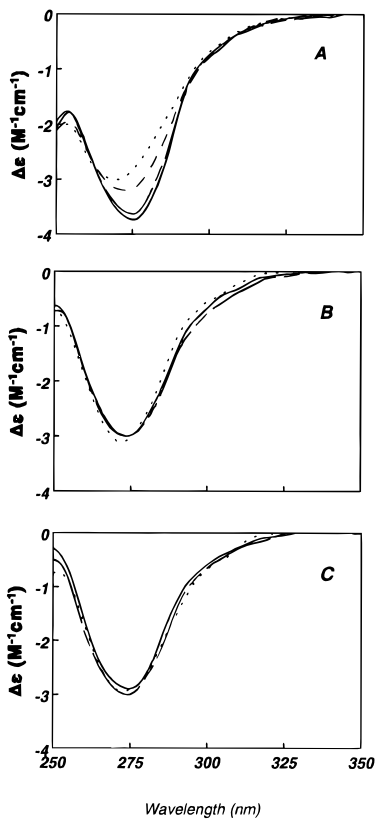

FIGURE 2: Near-UV CD spectra as a function of protein concentration. (A) Zinc-free human insulin in 10 mM Tris/ClO_4^-, pH 8.0, and (•••) 5 μM, (- - -) 20 μM, (- − -) 200 μM, and (—) 2 mM protein. (B and C) (B1, B10, B16, B27) Glu, des-B30 mutant insulin in 25 mM Tris/ClO_4^-, pH 7.5 (B), and 25 mM phosphate, pH 6.5 (C), and (•••) 50 μM, (- − -) 600 μM, and (—) 2.6 mM protein.

unusually broad, i.e., A8, A9, A12, B5, B6, and B26. The line width of the Cys A11 amide proton is unusually broad, but identification was possible in DQF-COSY spectra, although the cross-peak is below the threshold used in Figure 3A. Amide protons from residues A2, B6, and B9 were not identified. Finally, for the side chains of Glu and Gln residues, considerable overlap of cross-peaks in the $H^\beta-H^\gamma$ area was resolved using TOCSY spectra occasionally supported by NOESY.

Sequential Assignment and Secondary Structure. The sequential assignment was straightforward for most parts of the insulin mutant, including the regions B9−B29, A9−A12, and A13−A21. The assignment of the stretch from A4 to A8 was complicated by overlapping H^N and H^α resonances; this is reflected in the lack of sequential NOEs as well as NOEs indicative of secondary structure in this region. In the N-terminus of the B-chain, the NOEs are sparse, and the assignments here were made by exclusion as the very last part of the procedure.

The first indications of the secondary structures come from inspection of the chemical shifts of the α-protons compared to the random coil values (Wishart et al., 1992). These chemical shift differences shown in Figure 4 suggest helical structures characterized by upfield shifts of the α-protons in the second part of the A-chain [the A(II)-helix] and in the central part of the B-chain (the B-helix), whereas the helix expected in the N-terminus of the A-chain [the A(I)-helix] seems less well defined. These observations are substantiated by the NOEs assigned in the same regions as

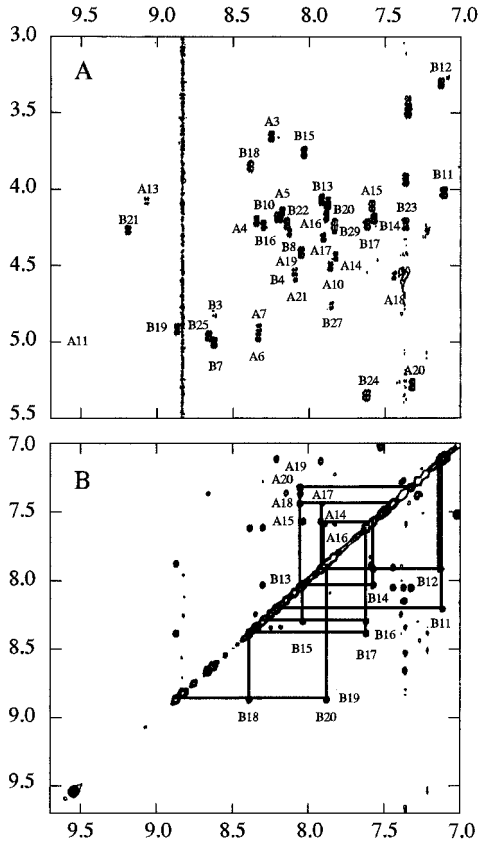

FIGURE 3: Sections from the DQF-COSY spectrum (panel A) and NOESY spectrum (mixing time 180 ms) (panel B). The fingerprint region of the DQF-COSY spectrum shows the major part of the correlations between α-protons and amide protons that was identified. The correlations between amide protons indicative of helical areas in the structure are annotated in the bottom panel, and lines are drawn to follow the amide protons throughout the A(II)- and B-chain helices.

shown in Figure 5 and in the NOE matrix in Figure 6. The B-helix, stretching from B9 to B19, is a well-defined helix characterized by a dense network of NOEs between the α-protons in position i and the amide protons in position $i + 3$ and position $i + 4$ as well as the β-protons in position $i + 3$. Furthermore, stronger NOEs between amide protons two residues apart in the helix are found. The C-terminal A(II)-helix comprising the amino acids from A13 to A20 has a less dense network of NOEs, i.e., only between α-protons in position i and β and amide protons in position $i + 3$. The N-terminal A(I)-helix stretches from A2 to A6 and is characterized by the same type of NOEs as the A(II)-helix. In the lower panel of Figure 3, the H^N to H^N part of the NOESY spectrum is shown with annotations for the sequential assignment of the helical areas.

An amide proton characterized by an exchange rate slower than the average is a good evidence for participation in a hydrogen bond either in a secondary structural element or as part of the tertiary fold of the protein. At near neutral pH, the exchange rate of amide protons is in the order of 10^2 min^{-1} (Englander et al., 1972). From 1D proton spectra recorded in the period between 12 and 60 min after dissolution of the insulin mutant in D_2O, it is possible by visual inspection to follow the decay of the resonances from several slow-exchanging amide protons belonging to the B-helix and the A(II)-helix as well as a single amide proton in the A(I)-helix. After 50 min, all amide protons are

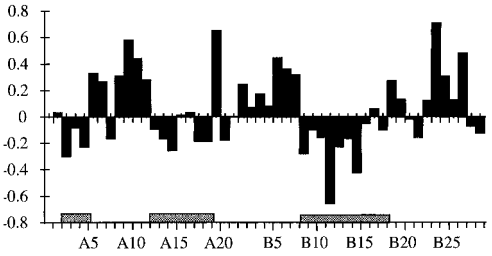

FIGURE 4: Difference between chemical shifts of the α-protons and the random coil values (Wishart et al., 1992). Stretches where the secondary chemical shifts indicate an α-helix are marked.

exchanged by deuterons. The locations of the slow-exchanging amide protons according to this criterion are shown in Figure 5.

Structure Calculations. Table 1 lists the number of distance restraints and dihedral angle restraints used for the final structure calculations. In addition, the sulfide bridges were added as distance restraints, while no restraints were added for hydrogen bonds. The matrix in Figure 6 shows the distribution of NOEs between residues. Multiple occurrences of NOEs from both sides of the diagonal in a spectrum or from different spectra were filtered out before the conversion of NOEs to distance restraints. The distribution of dihedral angle restraints on residues is shown in Figure 5. The calculation of structures using X-PLOR 3.0 proceeded as described in Materials and Methods starting from a reduced set of distance restraints. In a sequence of iterations, this set was slowly expanded as ambiguities could be resolved, and finally the dihedral angle restraints were introduced. A total of 100 structures were calculated, 25 of which were characterized by distance restraints violations below 0.3 Å, dihedral angle restraints violations below 2°, and a low total energy. Table 1 summarizes the structural statistics for this set of structures.

The geometric average of the set of 25 converged structures is shown in Figure 7; the average structure is colored according to the atomic rms deviation.

Description of the Structures. The major part of the mutant structure is well defined. This goes indeed for the B-helix (B9−B19) which exhibits low rms deviation among the structures as expected from the large number of structural NOEs as well as the small coupling constants, indicative of helix structure. The hydrogen bonds fit a regular α-helix pattern all the way starting from B9(CO)···B13(H^N) and ending at the last donor B19(H^N).

At the C-terminal end of the helix, a type I turn from B20 to B23 turns into a β-strand that stretches along the central helix. The three C-terminal residues are disordered. As is evident from Figure 5, no NOE structural information was obtained in the B1−B4 region of the B-chain. This fact is reflected in a random distribution of the termini among the 25 structures and implies that the average structure calculated in this area is physically meaningless. The A(II)-helix (A13−A20) shows a high degree of accordance within the bundle of structures, and the hydrogen bonding pattern fits an α-helix A13(CO)···A17(H^N), A15(CO)···A19(H^N), and A16(CO)···A20(H^N), starting out with the irregular A12-(CO)···A15(H^N) hydrogen bond. The A(I)-helix (A2−A8) is a little less well defined; a single hydrogen bond between A2(CO) and A6(H^N) is established. The loop area (A9−A12) connecting the two A-chain helices shows a larger spread of conformations. In 20 out of 25 calculated

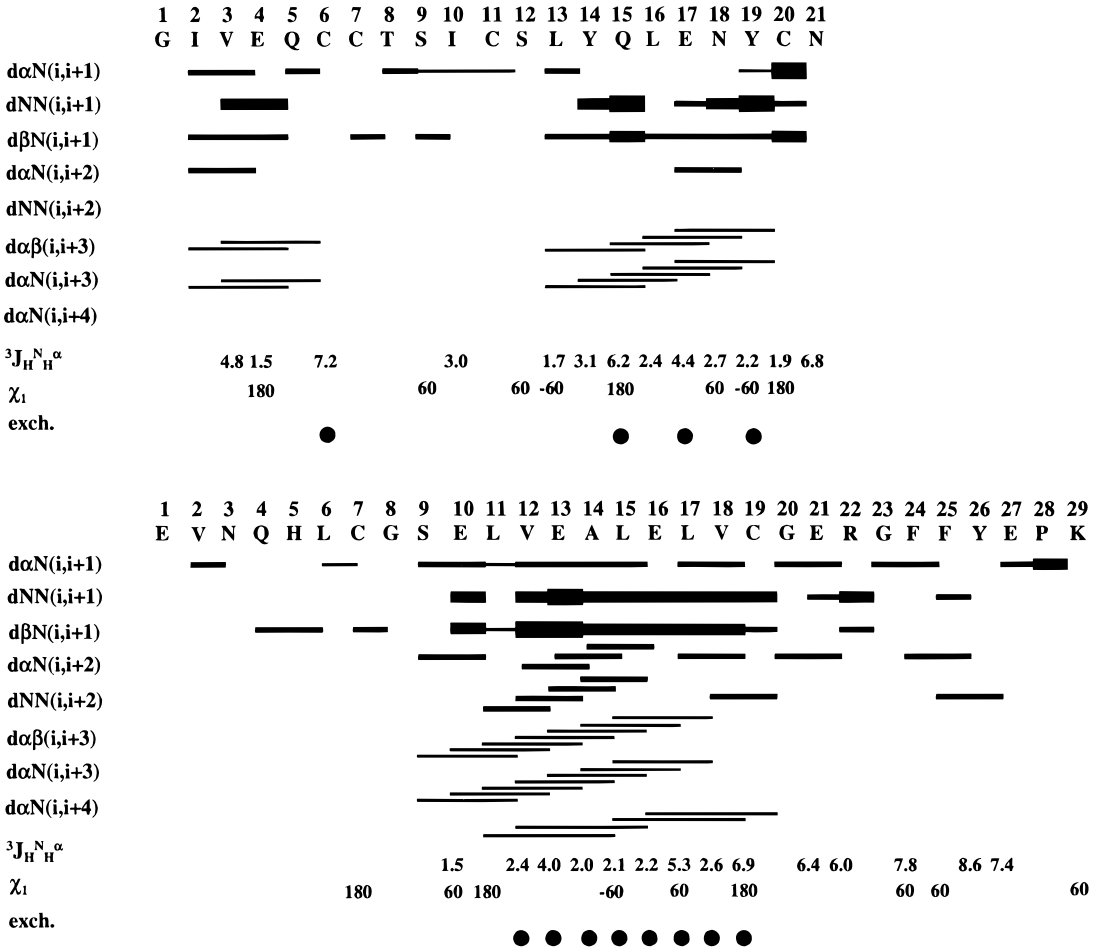

FIGURE 5: Summary of the data used for sequential assignment and determination of secondary structural elements. The thickness of the bars indicates the intensity of the NOEs as measured in a NOESY spectrum with a mixing time of 150 ms. The coupling constants and the χ_1 dihedral angles were measured as desribed in Materials and Methods. The filled circles indicate that the amide proton signal is observable in a 1D spectrum at least 12 min after dissolution of the sample in D_2O.

structures the interchain hydrogen bond A19(CO)···B25(H^N) is established, in agreement with crystal structures. The atomic rms deviations calculated are presented in Table 1 along with the general structural statistics.

DISCUSSION

The (B1, B10, B16, B27) Glu, des-B30 mutant is the first example of an insulin species that remains monomeric at millimolar concentration in aqueous solution at neutral pH. Hence, by tailored mutations in two distinct protein/protein interfaces, the inherent self-association of insulin is strongly inhibited, while the biological potency is only slightly reduced. As a result, samples may be prepared under conditions where the exchange rate of backbone amide protons is sufficiently slow for detailed NMR analysis. Previous NMR investigations of native and mutant insulins at near-neutral pH have been limited by incomplete assignments of the spectra. Nevertheless, on the basis of 1D spectra of human insulin at high dilution and of the B9 Ser → Asp monomeric mutant in the pH 8−9.5 range, Roy et al. (1990a,b) were able to show that the association of insulin monomers into dimers is accompanied by a change in conformation involving the relative position of residues B15 Leu and B24 Phe. In their NMR analysis of the B10 Asp, B28 Lys, B29 Pro (DKP) insulin monomer at pH 8.0, Weiss et al. (1991) also reported partial assignments and employed selective ^2H and ^{13}C labeling of the B23−B26 residues to confirm that this region is indeed in close contact with residues from the central B-chain helix.

The (B1, B10, B16, B27) Glu, des-B30 mutant is structurally well ordered with the exception of the B-chain termini, i.e., residues B1−B4 and B27−B29. The observed disorder in the N-terminus is most reasonably ascribed to opposing effects of the B1 and B10 mutations. Removal of the hydrophobic B1 Phe side chain destabilizes the packing of the B1 residue against the A13 Leu region (Ludvigsen et al., 1994), while the B10 Glu side chain caps the central B9−B19 helix and hence stabilizes the T-state relative to the R-state (Kaarsholm et al., 1993). In any event, because the B-chain helix is clearly confined to residues B9−B19, the overall structure resembles a crystallographic T-state more than an R-state. In the C-terminal B29−B30 residues, disorder is observed in the crystal structure as well as in the low-pH solution structure (Baker et al., 1988; Ludvigsen et al., 1994). In the present work at neutral pH, the lack of structural definition extends to the last three residues, B27−B29. Again, the effect is most likely due to the modifications employed, i.e., the introduction of negative charge close to the shortened C-terminus (B27 Thr → Glu, des-B30). In accordance with previous work (Kline & Justice, 1990; Ludvigsen et al., 1994), broad amide proton resonances are observed in the A-chain loop region, suggesting that conformational substates exchange on a millisecond time scale in this particular region.

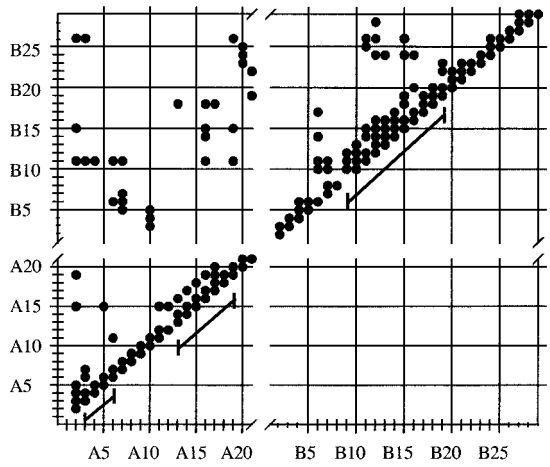

FIGURE 6: Overview of NOEs. Filled circles indicate the presence of at least one NOE between the connected residues. Multiple occurrences of NOEs on both sides of the diagonal in a spectrum or in different spectra were filtered out before the conversion to distance restraints. The presence of helical regions, as expected from the patterns of NOEs, is indicated.

Table 1: Structural Statistics for 25 Mutant Insulin Structures

Distances and Torsion Angle Restraints	
intraresidual 297	ϕ 34
short range 193	χ_1 14
long range 51	χ_2 5
cross chain 56	
Energy Statistics after Simulated Annealing (kcal/mol)	
total energy	43.8 ± 3.8
bonds	2.2 ± 0.2
angles	25.5 ± 2.2
repel	7.4 ± 1.2
NOE[a]	4.1 ± 1.3
torsion	0.3 ± 0.1
impropers	3.3 ± 1.3
van der Waals Energy Measured with CHARMM[b] Potential (kcal/mol)	
van der Waals	−70.4 ± 11.8
Deviations from Ideal Geometry	
bond (Å)	0.0017 ± 0.0001
angle (deg)	0.35 ± 0.02
improper (deg)	0.26 ± 0.04
NOE (Å)	0.012 ± 0.002
torsion (Å)	0.29 ± 0.05
Average No. of NOE Violations	
0.0−0.1 Å	31.8 ± 3.1
0.1−0.2 Å	2.0 ± 1.0
0.2−0.3 Å	0.16 ± 0.37
>0.3 Å	0
Atomic rms Values for 25 Converged Structures vs Their Geometric Average	
backbone (all)	1.31 ± 0.19
heavy atoms (all)	1.88 ± 0.23
backbone (A2−A19)[c]	0.67 ± 0.13
backbone (B4−B26)[c]	0.64 ± 0.09
backbone (A2−A19, B4−B26)[c]	0.66 ± 0.09

[a] Force constants for distance and torsion angle restraints are 50 kcal mol^{-1} Å^{-2} and 200 kcal mol^{-1} radian^{-2}. [b] CHARMM potential (Brooks et al., 1983) used for van der Waals energy calculation. [c] Alignment of A2−A19 and B4−B26 backbone.

Comparison with Other Monomer Solution Structures. Several NMR investigations of insulin monomers have been carried out at low pH and/or in the presence of organic cosolvent. Table 2 compares experimental conditions and details concerning the structure calculations for the (B1, B10, B16, B27) Glu, des-B30 mutant and for other insulin

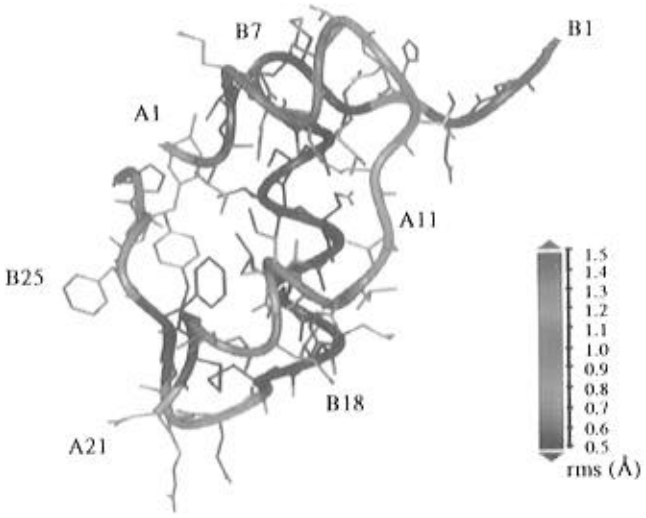

FIGURE 7: Geometric average structure of the insulin mutant colored according to atomic rms. The average structure was calculated on the basis of alignment of residues B4−B26 and A2−A19.

monomer structures deposited in the Brookhaven Data Bank. In addition to these monomers, the structure of a B9 Asp insulin dimer has been described (Jørgensen et al., 1992), and the low-pH structure of DPI has been determined by Knegtel et al. (1991) as well as by Hua et al. (1992a). Figure 8 compares the three-dimensional structure of (B1, B10, B16, B27) Glu, des-B30 insulin with those of the other monomers. The structures are color coded according to the atomic rms deviations characterizing each of these ensemble average structures. Table 2 contains details concerning the average structure calculations, alignment procedures, and rms deviations of the backbone calculated by using the same alignment procedure for all mutants. Note that, for certain parts of these structures, distance restraints containing information about secondary and tertiary fold have been either absent or very few in number. As a result, considerable atomic rms deviations are obtained which make the average structures physically meaningless in these parts colored red in Figure 8. Note that the absence of structural definition of the C-terminal B22−B30 residues is evident for both fully active (B24 Gly) and essentially inactive (B24 Ser) species, indicating no obvious correlation between biological activity and structural definition in this part of the molecule. Nevertheless, these results have been taken to imply that receptor binding must be accompanied by a major conformational change in the C-terminus of the B-chain (Hua et al., 1991, 1993b). Paradoxically, a distinct bulge appears on the C-terminal β-strand of the B24 Ser mutant structure.

The precision of the individual structures is quantified by the ensemble average rms deviations in Table 2. A comparison of the two columns of backbone rms deviations in the table reveals that most of the differences are caused by imprecision of the C-terminus of the B-chain. The B16 His structure shows the highest degree of overall accordance between the individual structures in the ensemble. In this case, the precision is directly correlated with the number of interresidual distance restraints used in the structure calculation. However, due to differences in the procedures for counting of the NOEs and for the translation of NOEs into distance restraints, the correlation between structural precision and the number of NOEs is generally not straightfor-

Table 2: Details of the Three-Dimensional Structures of Human Insulin and Mutants Determined by NMR[a]

mutations of human insulin	experimental conditions[b] pH	T (C°)	solvent	concn (mM)	structure calculations[c] NOE	φ	χ_1	χ_2	no. of structures	alignment procedure[d]	rms[e] (Å) bb	h	rms[f] (Å) bb	h	lit. ref
des-(B26−B30)	1.8	25	20% HAc/ 80% H_2O	?	368	?	10	0	15	A2−A19, B9−B19[g]	0.78	1.41	0.60	1.11	Hua et al., 1992a
B24 Ser	1.9	25	20% HAc/ 80% H_2O	1.5	323	27	14	0	10	A2−A19, B4−B19	1.76	2.30	0.70	1.18	Hua et al., 1993b
B24 Gly	1.9	25	20% HAc/ 80% H_2O	1.5	290	27	14	0	9[h]	A2−A19, B4−B19	3.01	3.53	0.67	1.13	Hua et al., 1991
des-B25	3.0	37	H_2O	4.6	368	10	0	0	20	A2−A20, B2−B28	0.87	1.58	0.65	1.31	Jørgensen et al., 1996
human insulin	1.9	25	20% HAc/ 80% H_2O	1	422	28	15	0	11	A2−A19, B4−B28	0.97	1.57	0.63	1.13	Hua et al., 1991
B16 His	2.4	24	H_2O	2.5	479	44	23	6	20	A2−A19, B4−B28	0.42	0.85	0.33	0.69	Ludvigsen et al., 1994
(B1, B10, B16, B27) Glu, des-B30	6.5	34	H_2O	3	300	34	14	5	25	A2−A19, B4−B26	0.59	1.16	0.52	1.07	present work

[a] Structures of monomeric human insulin and mutants of this were determined by NMR and are available in the Protein Data Bank, Brookhaven, January 1996. [b] The experimental conditions include pH, temperature, solvent, and insulin concentration. [c] The number of NOEs (intraresidual NOEs excluded) and the number of dihedral angle restraints used in the calculations. [d] The alignment procedures used in the original publication and reproduced in the ensemble averages. [e] The rms deviations listed are calculated as ensemble averages using similar alignments for all molecules; the basis has been backbone atoms (bb) and all heavy atoms (h), respectively. Alignment used A2−A8, A12−A19, and B5−B28 (−B23 for DPI) [−B27 for (B1, B10, B16, B27) Glu, des-B30]. [f] Alignment used A2−A8, A12−A19, and B5−B19. [g] Originally only the B-chain helix was aligned. In order to make this average structure comparable to the others, alignment of the A-chain has been added. [h] 11 structures were published; 9 were deposited.

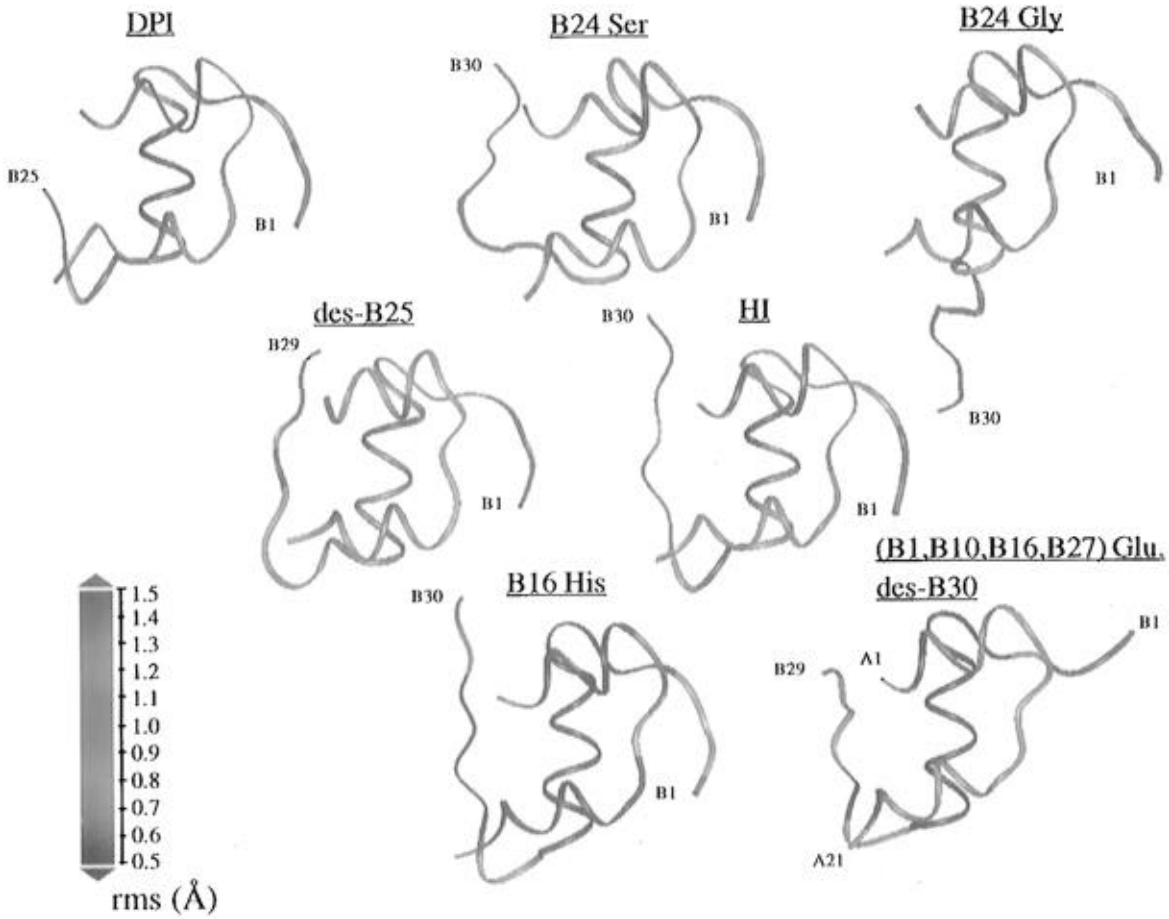

FIGURE 8: Ensemble averages of three-dimensional structures of native (HI) and mutant insulins determined by NMR. The structures are color coded according to the atomic root mean square deviation of the backbone. For further details, see Table 2.

ward. The high precision of side-chain structures in B16 His insulin are closely related to the number of stereospecific assignments of χ_1 and χ_2 dihedral angles. The individual monomer structures are compared one by one in Table 3. It is clear that the B16 His insulin has the closest structural resemblance to the (B1, B10, B16, B27) Glu, des-B30 mutant. The major difference between these two structures is the lack of definition of residues B1−B4 in (B1, B10, B16, B27) Glu, des-B30 insulin. In B16 His insulin, the close contact between the B-chain N-terminus and the A-chain loop region provides the set of NOEs defining the spatial arrangement of the loop. Thus, the lack of structure

Table 3: Comparison of Solution Structures of Human Insulin and Mutants[a]

	rms (Å)[a]						
	des-(B26−B30)	B24 Ser	B24 Gly	des-B25	human insulin	B16 His	(B1, B10, B16, B27) Glu, des-B30
des-(B26−B30)		1.07	1.38	1.26	0.33	1.12	1.15
B24 Ser	0.97		1.54	1.14	1.10	1.54	1.35
B24 Gly	1.41	1.54		1.36	1.37	1.14	1.18
des-B25	1.23	1.14	1.36		1.27	1.49	1.35
human insulin	0.33	1.10	1.37	1.27		1.09	1.08
B16 His	1.20	1.54	1.14	1.49	1.09		0.84
(B1, B10, B16, B27) Glu, des-B30	1.16	1.35	1.18	1.35	1.08	0.84	

[a] The root mean square deviations of the backbone were determined by aligning the regions A2−A19, and B4−B19 above the diagonal and the helix regions A2−A8, A13−A19, and B9−B19 below the diagonal. The structures are ensemble averages aligned as listed in Table 2.

in residues B1−B4 propagates to an increased imprecision of the A-chain loop region in (B1, B10, B16, B27) Glu, des-B30 insulin.

Finally, we note that, with the exception of the B-chain termini, the structures depicted in Figure 8 share common features, including the secondary structure elements and the overall spatial arrangement of these elements into the tertiary structure. As would be expected for a globular protein, Table 2 shows that each structural core is characterized by a low rms deviation (high precision) relative to the precision of the overall structure. In contrast with these calculations, Hua et al. (1992a, 1993a) reported that variations in the mutual spatial arrangement of the two chains in the case of DPI span the differences reported among various insulin crystal forms. The phenomenon was ascribed to the absence of restraints and interpreted as evidence that DPI exists in a "molten-globule" state under native-like conditions (Hua et al., 1992a, 1993a). A molten-globule state is usually characterized as a compact denatured state arising as an intermediate in the pathway from native to unfolded protein under slightly denaturing conditions [see, e.g., reviews by Dobson (1992, 1993)]. The state is characterized by the presence of secondary structural domains but the absence of tertiary interactions, i.e., the conformation of the side chains is essentially random. In an NMR spectrum, one feature of a molten globule state would be a reduced dispersion of side-chain resonances in comparison with the native state (Goto & Fink, 1989). The original alignment of the DPI ensemble presented by Hua et al. (1992a) was based on a subset of the structure, i.e., the central B-chain helix (residues B9−B19). This procedure per se leads to an accumulation of the overall structural imprecision in the parts that are left out of the alignment, in this case the entire A-chain and the B-chain termini. In contrast, our alignment procedure (Table 2) is based on both chains, leaving out only those parts of the molecule where the number of restraints per residue is well below the average, i.e., the outermost parts of both chains. The same procedure was used by Knegtel et al. (1991) for the alignment of DPI. With this procedure, the major part of all molecules (including DPI) exhibits reasonably well-ordered secondary and tertiary structure. For the (B1, B10, B16, B27) Glu, des-B30 mutant at neutral pH, and the B16 His mutant at low pH, the dispersion of side-chain resonances corresponds to that expected for a packed, globular protein. Furthermore, both mutants exhibit a distinct near-UV CD spectrum very similar to that of native human insulin [Figure 2 and Ludvigsen et al. (1994)]. Hence, there seems to be no evidence coming from NMR or CD to support the idea that insulin mutants exist in a molten-globule state characterized by variations in the mutual arrangement of the chains.

ACKNOWLEDGMENT

We thank I. Diers, S. Havelund, A.-M. Kolstrup, and L. G. Andersen for fermentation and purification of mutant insulins, A. R. Sørensen for insulin potency measurements, and A. Blom for assistance with operation and maintenance of the NMR spectrometer.

SUPPORTING INFORMATION AVAILABLE

Table of ^{1}H chemical shifts of the (B1, B10, B16, B27) Glu, des-B30 insulin mutant (1 page). Ordering information is given on any current masthead page.

REFERENCES

Adams, M. J., Blundell, T. L., Dodson, E. J., Dodson, G. G., Vijayan, M., Baker, E. N., Harding, M. M., Hodgkin, D. C., Rimmer, R., & Sheet, S. (1969) *Nature 224*, 491−496.

Anil-Kumar, Ernst, R. R., & Wüthrich, K. (1980) *Biochem. Biophys. Res. Commun. 95*, 1−5.

Anil-Kumar, Wagner, G., Ernst, R. R., & Wüthrich, K. (1981) *J. Am. Chem. Soc. 103*, 3654−3658.

Baker, E. N., Blundell, T. L., Cutfield, J. F., Cutfield, S. M., Dodson, E. J., Dodson, G. G., Hodgkin, D. M. C., Hubbard, R. E., Isaacs, N. W., Reynolds, C. D., Sakabe, K., Sakabe, N., & Vijayan, N. M. (1988) *Philos. Trans. R. Soc., Ser. B 319*, 369−456.

Bax, A., & Davis, D. G. (1985) *J. Magn. Reson. 65*, 355−360.

Bloom, C. R., Choi, W. E., Brzovic, P. S., Ha, J. J., Huang, S.-T., Kaarsholm, N. C., & Dunn, M. F. (1995) *J. Mol. Biol. 245*, 324−330.

Brader, M. L., Kaarsholm, N. C., Lee R. W.-K., & Dunn, M. F. (1991) *Biochemistry 30*, 6636−6645.

Brange, J., Ribel, U., Hansen, J. F., Dodson, G., Hansen, M. T., Havelund, S., Melberg, S. G., Norris, F., Norris, K., Snel, L., Sørensen, A. R., & Voigt, H. O. (1988) *Nature 333*, 679−682.

Braunschweiler, L., & Ernst, R. R. (1983) *J. Magn. Reson. 53*, 521−528.

Brooks, B. R., Bruccoleri, R., Olafson, B., States, D., Swaninathan, S., & Karplus, M. (1983) *J. Comput. Chem. 4*, 187−217.

Brünger, A. T. (1992) *X-PLOR manual version 3.0*, Yale University, New Haven, CT.

Crippen, G., & Havel, T. (1988) *Distance Geometry and Molecular Conformation*, Research Studies Press, Taunton, Somerset, England.

Derewenda, U., Derewenda, Z., Dodson, E. J., Dodson, G. G., Reynolds, C. D., Smith, G. D., Sparks, C., & Swensen, D. (1989) *Nature 338*, 594−596.

Dobson, C. M. (1991) *Curr. Opin. Struct. Biol. 1*, 22−27.

Dobson, C. M. (1992) *Curr. Opin. Struct. Biol. 2*, 6−12.

Englander, S. W., Downer, N. W., & Teitelbaum, H. (1972) *Annu. Rev. Biochem. 41*, 903−924.

Goldman, J., & Carpenter, F. H. (1974) *Biochemistry 13*, 4566−4574.
Goto, Y., & Fink, A. L. (1989) *Biochemistry 28*, 945−952.
Hua, Q. X., Shoelson, S. E., Kochoyan, M., & Weiss, M. A. (1991) *Nature 354*, 238−241.
Hua, Q. X., Kochoyan, M., & Weiss, M. A. (1992a) *Proc. Natl. Acad. Sci. U.S.A. 89*, 2379−2383.
Hua, Q. X., Shoelson, S. E., & Weiss, M. A. (1992b) *Biochemistry 31*, 11940−11951.
Hua, Q. X., Ladbury, J. E., & Weiss, M. A. (1993a) *Biochemistry 32*, 1433−1442.
Hua, Q. X., Shoelson, S. E., Inouye, K., & Weiss, M. A. (1993b) *Proc. Natl. Acad. Sci. U. S. A. 90*, 582−586.
Hybert, S. G., Märki, W., & Wagner, G. (1987) *Eur. J. Biochem. 164*, 625−635.
Jeener, J., Meier, B. H., Bachmann, P., & Ernst, R. R. (1979) *J. Chem. Phys. 71*, 4546−4553.
Jeffrey, P. D., & Coates, J. H. (1966) *Biochemistry 5*, 489−498.
Jeffrey, P. D., Milthorpe, B. K., & Nichol, L. W. (1976) *Biochemistry 15*, 4660−4665.
Jørgensen, A. M., Kristensen, S. M., Led, J. J., & Balschmidt, P. (1992) *J. Mol. Biol. 227*, 1146−1163.
Jørgensen, A. M., Olsen, H. B., Led, J. J., & Balschmidt, P. (1996) *J. Mol. Biol. 257*, 684−699.
Kaarsholm, N. C., & Ludvigsen, S. (1995) *Receptor 5*, 1−8.
Kaarsholm, N. C., Ko, H.-C., & Dunn, M. F. (1989) *Biochemistry 28*, 4427−2235.
Kaarsholm, N. C., Havelund, S., & Hougaard, P. (1990) *Arch. Biochem. Biophys. 283*, 496−502.
Kaarsholm, N. C., Norris, K., Jørgensen, R. J., Mikkelsen, J., Ludvigsen, S., Olsen, O. H., Sørensen, A. R., & Havelund, S. (1993) *Biochemistry 32*, 10773−10778.
Kadima, W., Roy, M., Lee, R. W.-K., Kaarsholm, N. C., & Dunn, M. F. (1992) *J. Biol. Chem. 267*, 8963−8970.
Kjaer, M., Andersen, K. V., Shen, H., Ludvigsen, S., Windekilde, D., Sørensen, B., & Poulsen, F. M. (1991) *NATO ASI Series* (Hoch, J. C., Redfield, C., & Poulsen, F. M., Eds.) Plenum, New York.
Kline, A. D., & Justice, R. M., Jr. (1990) *Biochemistry 29*, 2906−2913.
Knegtel, R. M. A., Boelens, R., Ganadu, M. L., & Kaptein, R. (1991) *Eur. J. Biochem. 202*, 447−458.
Kuszewski, J., Hilges, M., & Brünger, A. T. (1992) *J. Biomol. NMR 2*, 33−56.
Lord, R. S., Gubensek, F., & Rupley, J. A. (1973) *Biochemistry 12*, 4385−4392.
Ludvigsen, S., Andersen, K. V., & Poulsen, F. M. (1991) *J. Mol. Biol. 217*, 731−736.
Ludvigsen, S., Roy, M., Thøgersen, H., & Kaarsholm, N C. (1994) *Biochemistry 33*, 7998−8006.
Marion, D., & Wüthrich, K. (1983) *Biochem. Biophys. Res. Commun. 117*, 486−492.
Mark, A. E., Nichol, L. W., & Jeffrey, P. D. (1987) *Biophys. Chem. 27*, 103−117.
Markussen, J., Diers, I., Engesgaard, A., Hansen, M. T., Hougaard, P., Langkjaer, L., Norris, K., Ribel, U., Snel, L., Sørensen, A. R., Sørensen, E., & Voigt, H. O. (1987) *Protein Eng. 1*, 215−223.
Moody, A. D., Stan, M. A., Stan, M., & Gliemann, J. (1974) *Hormone Metab. Res. 6*, 12−16.
Morris, J. W. S., Mercola, D., & Arquilla, E. R. (1968) *Biochim. Biophys. Acta 160*, 145−155.
Nilges, M., Clore, G. M., & Gronenborn, A. M. (1988) *FEBS Lett. 139*, 317−324.
Pekar, A. H., & Frank, B. H. (1972) *Biochemistry 11*, 4013−4016.
Piantini, U., Sørensen O. W., & Ernst, R. R. (1982) *J. Am. Chem. Soc. 104*, 6800−6801.
Pocker, Y., & Biswas, B. (1981) *Biochemistry 20*, 4354−4361.
Rance, M., Sørensen, O. W., Bodenhausen, G., Wagner, G., Ernst, R. R., & Wüthrich, K. (1983) *Biochem. Biophys. Res. Commun. 117*, 479−485.
Roy, M., Lee, R. W. K., Brange, J., & Dunn, M. F. (1990a) *J. Biol. Chem. 265*, 5448−5452.
Roy, M., Lee, R. W.-K., Kaarsholm, N. C., Thøgersen, H., Brange, J., & Dunn, M. F. (1990b) *Biochim. Biophys. Acta 1053*, 63−73.
Smith, G. D., Swenson, D. C., Dodson, E. J., Dodson, G. G., & Reynolds, C. D. (1984) *Proc. Natl. Acad. Sci. U.S.A. 81*, 7093−7097.
Strazza, S., Hunter, R., Walker, E., & Darnall, D. W. (1985) *Arch. Biochem. Biophys. 238*, 30−42.
Strickland, E. H., & Mercola, D. (1976) *Biochemistry 15*, 3875−3884.
Wagner, G., Braun, W., Havel, T. F., Schaumann, T., Gõ, & Wüthrich, K. (1987) *J. Mol. Biol. 196*, 611−639.
Weiss, M. A., Hua, Q.-X., Lynch, C. S., Frank, B. H., & Shoelson, S. E. (1991) *Biochemistry 30*, 7373−7389.
Wishart, D. S., Sykes, B. D., & Richards, F. M. (1992) *Biochemistry 31*, 1647−1651.
Wood, S. P., Blundell, T. L., Wollmer, A., Lazarus, N. R., & Neville, R. W. J. (1975) *Eur. J. Biochem. 55*, 531−542.
Wüthrich, K. (1986) *NMR of Proteins and Nucleic Acids*, Wiley, New York.

BI960292+